buildings

MDPI

Article

A Study of the Mechanical Behavior of a Steel–Concrete Hybrid Beam Bridge during Construction

Huiteng Pei [1,2], Lijun Jia [1], Jiawei Li [1], Kewei Li [1] and Ruijie Xia [3,*]

[1] Department of Bridge Engineering, College of Civil Engineering, Tongji University, Shanghai 200092, China; 2180098@tongji.edu.cn (H.P.); jialj@tongji.edu.cn (L.J.); 2132367@tongji.edu.cn (J.L.); 2232314@tongji.edu.cn (K.L.)
[2] Jiangxi Communication Design and Research Institute Co., Ltd., Nanchang 330052, China
[3] Shanghai Municipal Engineering Design Institute (Group) Co., Ltd., Shanghai 200092, China
* Correspondence: xiaruijie@smedi.com

Abstract: To study the mechanical properties of steel–concrete joints during construction, the Mao Port Bridge in Shanghai is used as a case study. The mechanical properties of the bridge and the joint under the construction conditions were studied based on the site construction monitoring results, the finite element calculation of the entire bridge and the refined model of the joint. The results show that the finite element analysis of the bridge and the stress analysis of the joint during the construction phase agreed with the measured values, the end of block 0# of the main span remained in compression during construction and the compressive stresses varied in a zigzag pattern with the progress of construction. The lifting of the mid-span steel beam is a critical construction condition where the side spans of the girders are stretched upwards by 20.9 mm and the main spans are stretched downwards by 32.3 mm. When the steel beam was lifted, the joint was compressed as a whole. At the joint, the longitudinal stresses in the steel structure gradually decreased from the front bearing plate to the joint face, while the longitudinal stresses in the concrete structure gradually increased.

Keywords: steel–concrete joint; hybrid continuous beam; construction process; on-site monitoring; mechanical behavior

Citation: Pei, H.; Jia, L.; Li, J.; Li, K.; Xia, R. A Study of the Mechanical Behavior of a Steel–Concrete Hybrid Beam Bridge during Construction. *Buildings* **2023**, *13*, 1781. https://doi.org/10.3390/buildings13071781

Received: 20 June 2023
Revised: 3 July 2023
Accepted: 4 July 2023
Published: 13 July 2023

1. Introduction

A steel–concrete hybrid beam bridge is a bridge where mid-span concrete beams are replaced with steel beams, which reduces the weight of the bridge. This type of structure is increasingly used in practical engineering because of its many benefits.

He et al. [1] suggested a method to determine the reasonable length of steel beams during the preliminary design phase of steel–concrete hybrid beam bridges. The method establishes its relationship with the length ratio between the side span and the main span and solves the reasonable length ratio between the steel structure part and the main span explicitly.

The steel–concrete joint of a hybrid beam is a crucial component that has been extensively researched. For the mechanical performance of a joint, the stress situation and internal force sharing ratio of each member were investigated by finite element modeling of the joint [2–4]. The results showed that the joint could easily transfer internal forces thanks to the major internal force-bearing elements, bearing plate and shear connector. Scale tests are also widely used to study joint force. Chen et al. [5] conducted a 1:2 scale test on the steel–concrete joint of the Taozhaomen Bridge and analyzed the mechanical performance of the joint combined with the finite element model. Huang et al. [6] conducted a 1:3 scale model test on the joint of a three-tower hybrid beam cable-stayed bridge for analyzing its bearing performance under different load conditions and the stress distribution of steel and concrete members within the joint. Qin et al. [7,8] studied the reasonable location of a steel–concrete joint surface of a hybrid beam bridge based on the finite element method

taking Weihe Bridge as the background, and later, they designed a scale test model with a similarity ratio of 1:3 for the special railway bridge in Chongqing, tested the stress and the slip of the model, and compared the test results with the finite element analysis results. Yao et al. [9] took the steel–concrete joint of Yongjiang Great Bridge as the research object and conducted a full-section scale test and finite element analysis with a similar ratio of 1:5 to investigate the normal stress distribution and bearing capacity of a steel–concrete joint under normal service, overload and failure conditions. Cheng et al. [10] tested and theoretically analyzed the longitudinal force transfer mechanism of a steel–concrete joint of a hybrid beam cable-stayed bridge through five full-size local structural specimens. Wei Feng et al. [11] studied the mechanical performance of the back bearing plate joint of a cable-stayed bridge without a lattice chamber by combining real bridge stress detection and finite element analyses and found that the compressive stress level was low in the whole test process at the joint section and its adjacent beam sections.

Because of the complexity of steel–concrete joint structures, many scholars have studied them from the perspective of geometric construction. Kulkarni et al. [12] carried out a nonlinear finite element analysis of a joint, considering the influence of axial load, the thickness of the connecting plate and the continuation of reinforcement at the bottom of the beam on its stress. Zhang et al. [13] combined theoretical calculation and finite element simulation to discuss the influence of factors such as the length of the joint and the stiffness of the shear connector. Kim et al. [14,15] conducted experimental studies on three types of joints on small steel–concrete hybrid beams to determine the joint types suitable for a hybrid beam bridge and conducted full-scale model tests on a new joint type to verify its effectiveness. Xin et al. [16] carried out an experiment on the ultimate bearing capacity and buckling modes of five different steel stiffening segments in a hybrid structure and compared the results with the finite element ones. Liu et al. [17] studied the auxiliary ribs of a steel–concrete joint and found that the auxiliary ribs dispersed approximately 50% of the axial force, which improved the stress transfer of the joint. He et al. [18–21] first conducted experiments on a joint with a new connect method using perfo-bond strip (PBL) connectors to investigate the reliability and safety of the method. Then, based on the tests of 12 PBL specimens, the connector behavior was discussed, including the failure mode, ductility and the components of ultimate shear strength. The mechanical properties of PBL joints after UHPC had replaced ordinary concrete were also studied. The results showed that the steel–UHPC joints had good combined properties and sufficient strength.

In addition, some relevant studies from a dynamics perspective have been conducted. Liu et al. [22] analyzed the stiffness ride of a joint from the perspective of dynamics. Through on-site tests and numerical analysis, Li et al. [23] evaluated the dynamic performance of a steel–concrete hybrid beam bridge with spread steel box beam under vehicle loads, and the results showed that the maximum impact coefficient of the bridge met the Chinese and American bridge design codes. Zhang et al. [24] conducted an experimental study on hybrid beams from the perspective of seismic resistance and found that the failure mode of precast hybrid beams was different from that of precast concrete beams. Lu et al. [25] carried out a finite element analysis on the fatigue performance of an important component of the joint, shear connectors.

Thus, existing research mainly focuses on the testing and numerical simulation of the mechanical properties of joints in hybrid beams. There are few studies of the mechanical properties of a steel–concrete hybrid beam bridge during construction and monitoring stages of the actual bridge. In this paper, we establish a hybrid beam space model based on Midas Civil and a refined model of the joint based on ANSYS using the engineering background of the Shanghai Damemao Port Bridge. By combining these models with results from real bridges, we study the mechanical behaviors of a hybrid continuous beam bridge during the construction stage and discuss the mechanical properties of the steel–concrete joint in the construction process.

2. Background

The Mao Port Bridge is a three-span continuous hybrid beam bridge with three lanes in each direction. It has a single span width of 16 m and a span arrangement of 65 m + 135 m + 65 m. The bridge has a box cross-section with a single cell for the main beam. The middle span of the bridge includes two 40 m concrete beams and a 55 m steel beam. The middle 50 m of the steel beam is the hoisting section, with 2.5 m on both sides as the connection segment. Both ends of the steel box beam are connected to the concrete segment through a 4 m long joint. The joint adopts a combination of front and back bearing plate construction and lattice chamber, as shown in Figures 1–3.

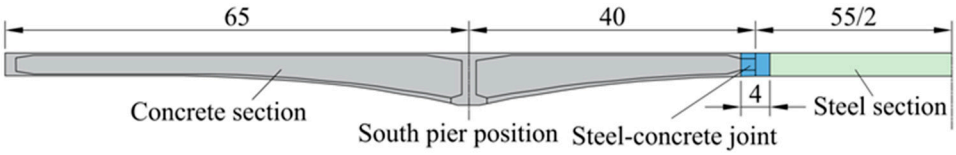

Figure 1. Profile diagram of the bridge (m).

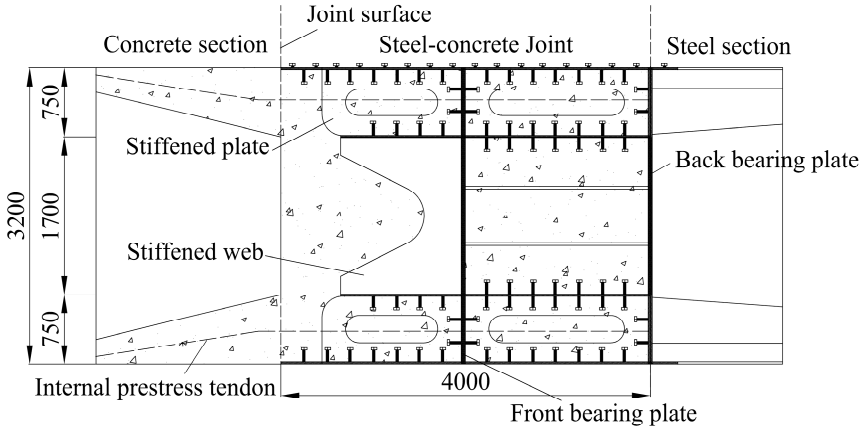

Figure 2. Longitudinal section of the joint (mm).

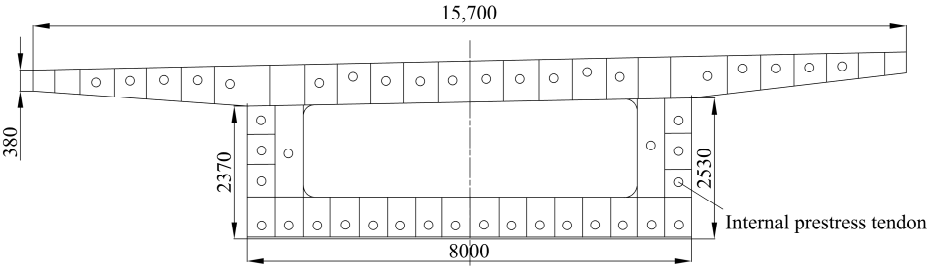

Figure 3. Cross-section of the joint (mm).

3. Monitoring Program

3.1. Vertical Displacement Measuring Point Location

In order to analyze the mechanical behavior of the structure in real time, the deformations and stresses in key sections of the bridge were monitored during the construction of this hybrid continuous beam bridge. A total of 47 sections of the main beam were selected for displacement monitoring. The southern part of the bridge is shown in Figure 4 with section numbers 1~23, while for the northern part, the same sections were assigned section numbers 1′~23′. A total station (Leica TS30) was used to monitor the vertical displacements of the main beams and piers, and two prisms were placed symmetrically in each monitoring section. The locations of the measuring points of some sections are shown in Figure 5.

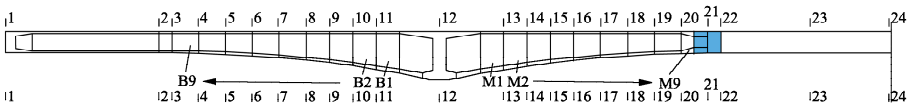

Figure 4. Longitudinal arrangement of the displacement measuring points of the main beam.

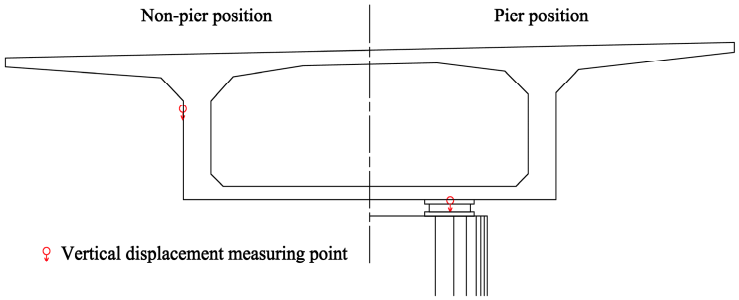

Figure 5. Transverse arrangement of the displacement measuring points in some sections.

3.2. Longitudinal Stress Measuring Point Location

A total of 12 stress monitoring sections were selected, as shown in Figure 6, and some of the stress measuring points were arranged as shown in Figures 7–9.

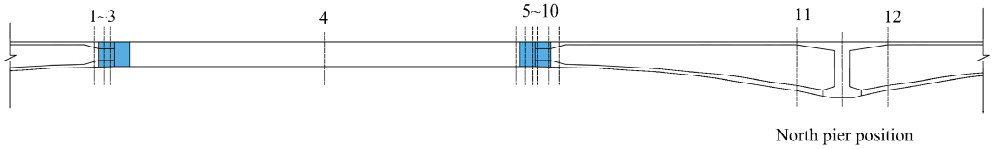

Figure 6. Longitudinal arrangement of stress monitoring section.

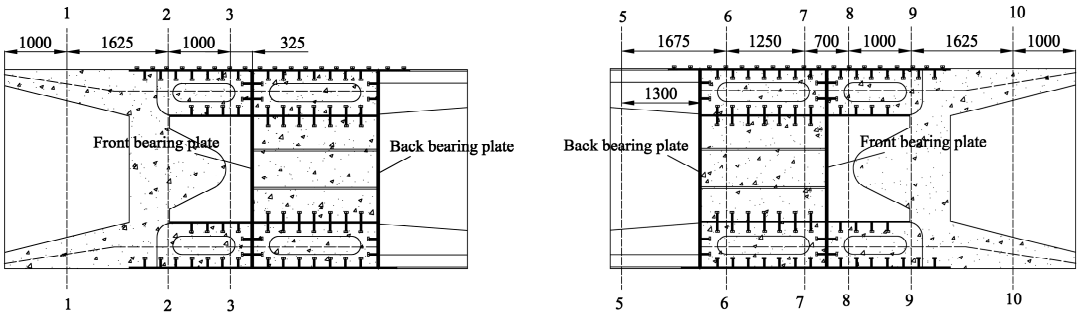

Figure 7. Stress monitoring section in the joint. (**a**) sections 1-1~3-3 arrangement (mm). (**b**) sections 5-5~10-10 arrangement (mm).

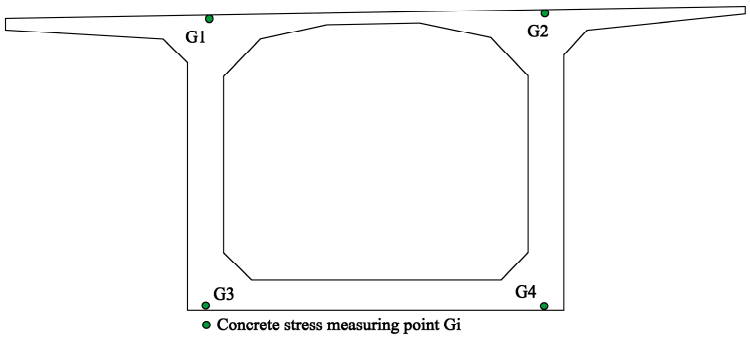

Figure 8. Stress measuring points of concrete sections 11-11 and 12-12.

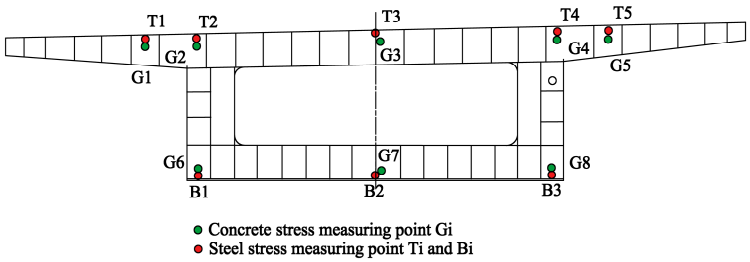

Figure 9. Stress measuring points of joint sections 8-8 and 9-9.

3.3. Measurement of Construction Conditions

The construction process was divided into 29 conditions for the monitoring, as shown in Table 1. A single measurement was taken before and after the construction of each condition, and the difference between the two measurements was taken as the deformation of the main beam under that construction condition.

Table 1. Construction conditions.

Construction Condition	Content	Construction Condition	Content	Construction Condition	Content
1	Main pier construction	12	Block 5# pouring	23	T10/Z1~Z3/ZH1~ZH5 tension
2	Block 0# pouring	13	F10/T6/T11 tension	24	Side span straight section cast-in-place
3	F1/F2/T1 tension	14	Block 6# pouring	25	Side span closing section cast-in-place
4	Block 1# pouring	15	F11/T7/T12 tension	26	B1~B4/BH1/BH2 tension
5	F3/F4/T2 tension	16	Block 7# pouring	27	Hoisting of mid-span steel beam
6	Block 2# pouring	17	F12/T8 tension	28	Y1/Y2 tension
7	F5/F6/T3 tension	18	Block 8# pouring	29	Bridge deck pavement
8	Block 3# pouring	19	F13/T9 tension		
9	F7/F8/T4 tension	20	Block 9# pouring		
10	Block 4# pouring	21	F14 tension		
11	F9/T5 tension	22	Site joint section pouring		

Note: F*/ZH*—web prestressed tendons; T*/BH*—top plate prestressed tendons; Z*/B*—bottom plate prestressed tendons; Y*—external prestressed tendons. Block *#—concrete block B* and M* in Figure 4. "*" means a number.

4. Analysis of the Mechanical Behavior of the Main Beam

The deformation of the main beam and the stress of some key sections under each construction condition was monitored on the site. A finite element model of the hybrid beam bridge was created to study the mechanical behavior of the bridge during construction, and a refinement finite element model of the steel–concrete joint was created for the mechanical properties of the joint.

4.1. Finite Element Model of the Hybrid Beam Bridge

MIDAS Civil was used to establish the spatial finite element model of the hybrid beam bridge. In the model, the main beam was modeled by the beam unit and the longitudinal prestress tendons in the concrete were added by setting steel bundles and tension prestress; the external prestress was simulated by a truss unit with initial tension. C55 was used for concrete and Q345qd was used for steel.

The bridge was constructed by cantilever casting with a hanging basket. The main bridge block 0# was constructed by a cantilever supporting frame and blocks 1# to 9# were cast by hanging basket cantilever. At this time, the middle pier was temporarily cemented; thus, six degrees of freedom of the 0# block were restrained. The cast-in-place segment of the side span was constructed using the full-span bracing method, which was simulated in the model by adding only pressure-bearing units. The first system conversion was carried out after the side span was closed. The temporary consolidation of the middle pier was released and the longitudinal freedom of the bearing on the middle pier was restrained. The second system conversion was performed to achieve the final restraint state after the completion of the hoisting and welding of the steel beam section in the middle span and before external prestress tension. The calculation considered the self-weight and the second phase of dead load. The finite element model is shown in Figure 10.

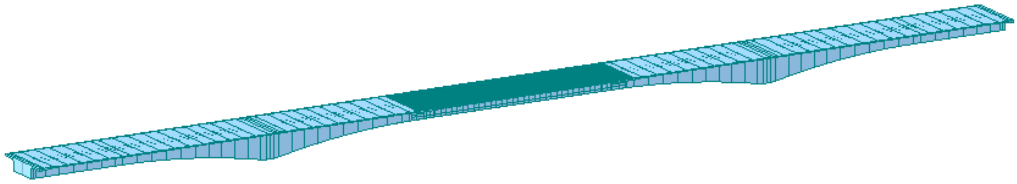

Figure 10. Finite element model of the bridge.

4.2. Deformation Analysis of the Hybrid Beam in Each Construction Process

For the site monitoring, since the deformation of the section monitored under construction conditions 2–11 was not clear enough, monitoring commenced from working condition 12. At the same time, in order to analyze the deformation of the main beam in the whole construction stage more comprehensively, sections 8′-8′ and 9-9 of the middle side span and sections 17-17 and 18′-18′ of the middle span in Figure 4 were selected for analysis.

The finite element calculation results are shown in Figure 11. It shows that the main beam deflection went up and down according to the construction condition, and the main beam section was deflected downward during the concrete casting stage and upward during the prestress tendon tensioning stage. In condition 22, since sections 18′-18′ and 17-17 were located at the mid-span, pouring the field connection made the deflection of these two sections more clear than that of sections 8′-8′ and 9-9. Conditions 24 and 25 showed the casting of the straight segment and the casting of the jointed segment, respectively, on the side span, and almost no deformation occurred in the main beam at this stage. For condition 26, since sections 8′-8′ and 9-9 were in the side span, tensioning the prestress tendons in the side span made the two sections deflect down, while it had little effect on sections 18′-18′ and 17-17, which were in the middle span. In condition 27, sections 18′-18′ and 17-17 deflected downward, while sections 8′-8′ and 9-9 deflected upward, and the deformation values of both downward and upward deflection were large. Because of the large self-weight of the steel beam segment on the middle span, the hoisting of the steel beam on the middle span caused a large downward deflection of the two sections on the middle span and a large upward deflection of the two sections on the side span. But the section deflection was controlled after tension of prestress tendons in condition 28.

As the construction process progressed, the deformation of conditions 12 to 26 was more stable, while the deformation of the main beam under condition 27 was larger. The deformation was controlled after tensioning the prestress tendons in working condition 28. The measured and calculated values of displacement of partial sections in conditions 27 and 28 are shown in Figure 12.

In condition 27, the measured value of each section of the main beam on the south pier was approximately the same as the calculated value; the difference between the two was not more than 5 mm. The maximum measured upper deflection value on the side span was 20.9 mm and the maximum measured lower deflection on the middle span was −32.3 mm. In working condition 28, the measured values of each section of the main beam on the north pier differed from the calculated values, but the deformation of the main beam was

low, with differences all within 5 mm, and the maximum difference between the two was only 0.9 mm. A possible reason for this is the lack of precise measurement.

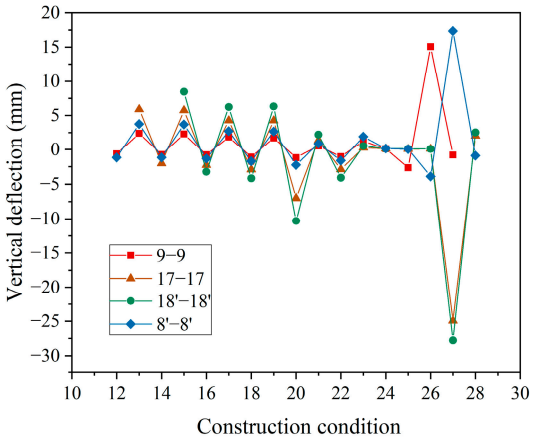

Figure 11. Calculated construction displacement diagram of key sections.

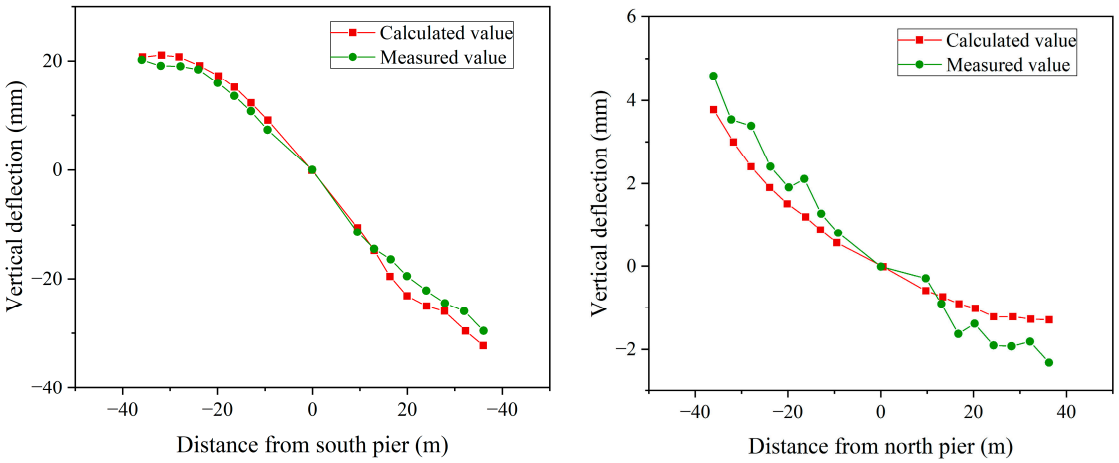

Figure 12. Deflection of main beam under key construction conditions. (**a**) Comparison of measured and calculated deflections of the main beam of the south pier in condition 27. (**b**) Comparison of measured and calculated deflections of the main beam of the north pier in condition 28.

4.3. Stress Analysis of the Hybrid Beam in Each Construction Process

The most unfavorable stress part of the main beam in the cantilever construction was located at the root of the cantilever; thus, the stress change of the hybrid beam in the construction stage was analyzed by focusing section 11-11 at the end of the mid-span of block 0#. The measured value of stress variation in the parallelogram direction of section 11-11 during the processes of casting and hoisting the steel beam onto the mid-span and the calculated value of stress variation are shown in Figure 13.

During cantilever casting and the hoisting of the steel beam onto the mid-span, the values of stress variation in the top plate of section 11-11 were both positive and the values of stress variation in the bottom plate were both negative. This indicates that the tensile stress in the top plate and compressive stress in the bottom plate continued to increase near the root of the cantilever on the mid-span during the concrete casting and steel beam hoisting phases. From conditions 6 to 20, the overall trend of stress variation in the top plate rose and the overall trend of stress variation in the bottom plate decreased, which was because the casting segment was gradually moving away from the root of the cantilever and the bending moment effect brought by the self-weight was becoming more and more significant. At condition 20, the stress variation was the largest, with a measured stress

variation value of 1.71 MPa in the top plate and −2.12 MPa in the bottom plate. Due to the low self-weight of the connection section, the value of the bending moment was small, resulting in a smaller value of its stress variation in condition 22. The stress variation value in condition 27 became larger when hoisting the steel beam onto the mid-span due to the heavy self-weight of the steel beam. The measured values of stress variation in the top and bottom plates were all located near the curve of the calculated values, and the maximum difference was 0.29 MPa.

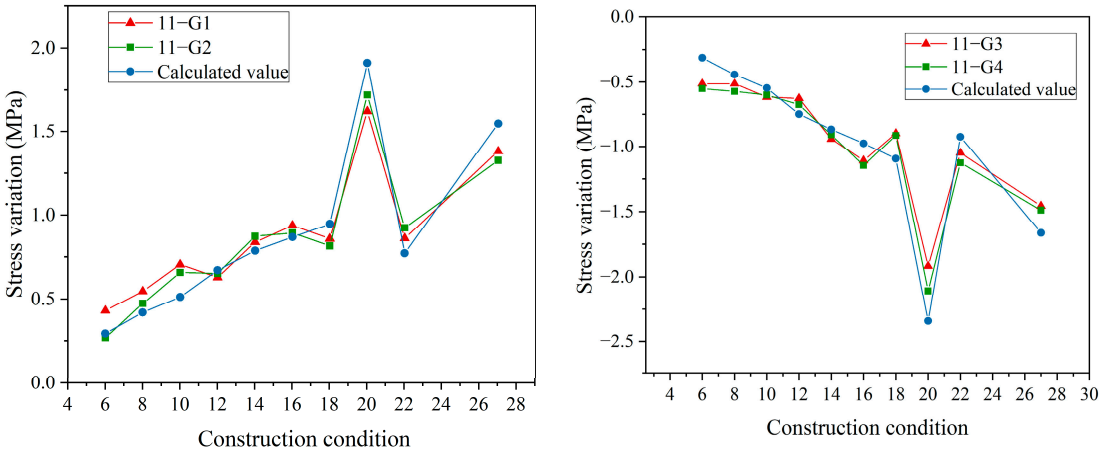

(**a**) (**b**)

Figure 13. Stress variation of section 11-11 (MPa). (**a**) Top plate. (**b**) Bottom plate.

Figure 14 shows that the cumulative stress in the top and bottom plates of section 11-11 in each construction stage presented a sawtooth-shaped change, which was due to the alternate push of the cast segment and tension stress during the construction process. During the construction process, no tensile stress appeared at each measurement point in the end section of block 0#, and a maximal compressive stress appeared in the top plate of section 11-11 in condition 21.

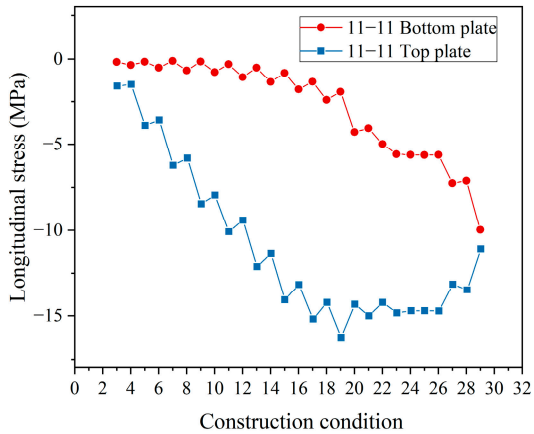

Figure 14. Calculated values of stress in monitored section 11-11.

5. Analysis of the Mechanical Properties of the Steel–Concrete Joint

5.1. Finite Element Model of the Joint

In order to investigate the mechanical properties of the joint during the construction process, the stress state of joint sections 8-8 and 9-9 during the hoisting of the steel beam and the closure of the mid-span (condition 27) was selected for analysis. Using ANSYS, a local finite element model was established for the joint section of the bridge. The longitudinal

length of the model was 16 m, including a 6 m concrete beam, 4 m joint, 2.5 m steel beam stiffened transition section and 3.5 m steel beam section.

In the model, the Shell 181 unit was selected for the steel plate, Solid 65 unit was used for the joint concrete, Link 8 unit was used to simulate both the longitudinal prestress tendons and the vertical prestress tendons in the joint, and the linear axial spring unit Conbin14 was used to simulate the weld studs and PBL in the joint. The model cells were all divided in the form of a free mesh, the steel plate cells were divided into a quadrilateral mesh and the concrete cells were divided into a tetrahedral mesh. The effect of prestress tendons on the structure was mainly at the location of anchorage points; thus, each prestress tendon was divided into only one line cell. Since the structural forces were strictly detected and controlled during the construction, the materials were not considered to yield or fracture.

As for the force transmission between the steel structure and concrete in the joint, only the roles of the bearing plate and the joint were considered, ignoring the frictional transmission between them, allowing for results with a certain safety reserve. In the simulation, the concrete body was separated from the steel face and the concrete was fully coupled with nodes of the bearing plate. Spring units were established between the concrete and steel nodes as connections. Considering the large stiffness and small deformation of the concrete section, the model structure was made to form a single cantilever system by restraining the node for 6 degrees of freedom of the concrete beam end section. A master node was established at the location of the form center in the end plane of the steel beam, given the Mass unit, and a constraint equation was used to connect the master node to the other nodes of the section to form a rigid domain. The internal force values of the loading section of the steel beam in condition 27 were calculated from the full bridge finite element model in Midas Civil and applied to the master node as the internal force boundary conditions at the end of the steel beam. The connection between the prestress tendons and the concrete was achieved by using displacement restraint equations. Constraints were applied to the nodes at the ends of the prestress tendons and at the steering blocks, and the tensioning process was simulated by assigning initial strains to the prestress tendon units. The finite element model of the joint is shown in Figure 15.

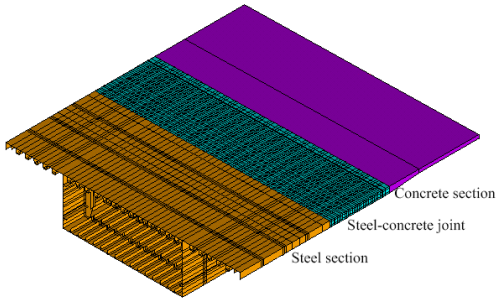

Figure 15. Finite element model of the joint.

5.2. Steel Stress Analysis of the Joint

Figure 16 shows the stress distribution of the steel structure in the parallelogram direction in condition 27. A stress concentration occurred in a small area where the bottom plate met the web in the boundary section of the steel beam, resulting in a high-stress level at this location. The stress of the rest was between −30 MPa and 32.11 MPa and the overall stress level was low, and much less than the design strength for the Q345qD steel of 270 MPa. The overall steel structure of the joint was in a compressed state. The bottom plate of the stiffened transition section of the steel beam exhibited tensile stress.

Figure 17 shows the measured and calculated values of stresses in the parallelogram direction of the steel structure in sections 8-8 and 9-9 from Figure 7 under condition 27. As can be observed from the figure, the error between the measured and calculated stresses in the parallelogram direction of the top and bottom slabs in sections 8-8 and 9-9 did not exceed 15%, which indicated the proper fitting. The calculation results show that the

transverse stresses in the top and bottom plates of both sections were symmetrical around the centerline of the main beam. The transverse distribution of the transverse stresses in the same cross-section varied greatly. The transverse distribution of the stresses in the top plate showed a multi-peak pattern. The maximum value of the stress of the top plate in section 8-8 in the parallelogram direction was located at the center line of the beam, while the stress at the edge of the section was the smallest. The rate of stress change near this location was significant, and the maximum difference between the measured and calculated values was 0.62 MPa. The stress distribution pattern of the top plate in section 9-9 was different from that in section 8-8. With the increase in the distance from the centerline of the beam, the stress in the parallelogram direction of the section increased and then decreased. The distribution was more uniform after reaching the web and, finally, the stress decreased rapidly near the edge of the section. The maximum difference between the measured and calculated values was 0.65 MPa. The transverse distribution of stresses in the bottom plate in sections 8-8 and 9-9 was nearly the same, with the stresses gradually increasing from the centerline of the beam to the vicinity of the stiffened web and rapidly decreasing from the stiffened web to the edge of the bottom plate. The maximum difference between the measured and calculated stresses in the bottom slab of sections 8-8 and 9-9 was 0.75 MPa and 0.35 MPa, respectively. Along the longitudinal direction of the bridge span, the stresses in the top and bottom plates of the steel structure gradually decreased from sections 8-8 to 9-9.

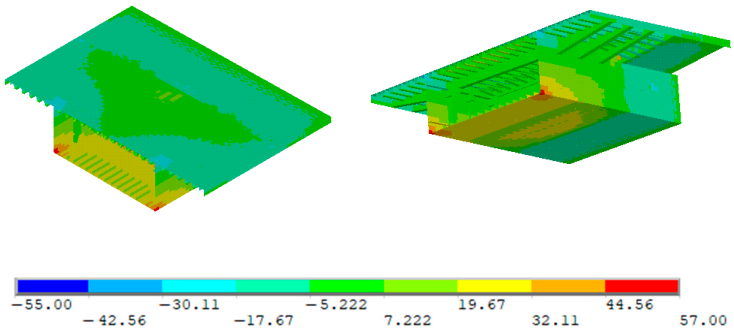

(**a**) (**b**)

Figure 16. Stress distribution in the parallelogram direction of the steel structure (MPa). (**a**) View from top. (**b**) View from bottom.

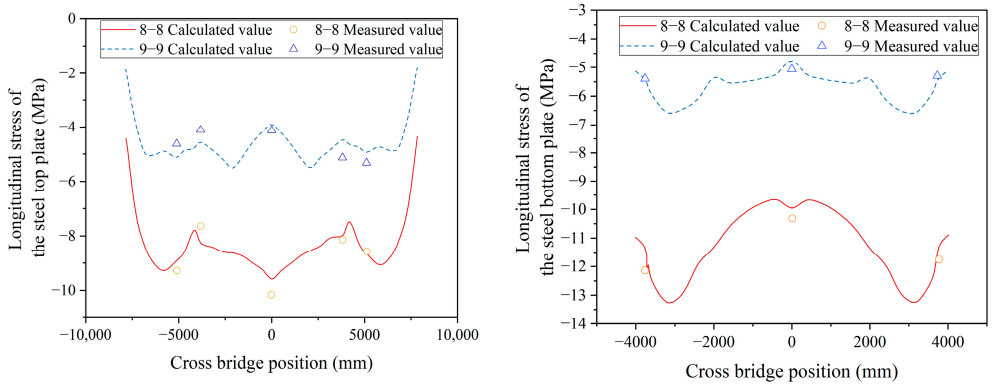

(**a**) (**b**)

Figure 17. Transverse distribution of the steel stress in cross sections (MPa). (**a**) Steel top plate stress. (**b**) Steel bottom plate stress.

5.3. Concrete Stress Analysis of the Joint

As for the concrete stresses, the monitored sections were in a compressed state in condition 27, not counting the stress concentrations generated by the anchorage of prestress

tendons. Stress in section 1-1 was mainly distributed between −7.93 MPa and −2.04 MPa, stress in section 2-2 was mainly distributed between −4.34 MPa and −1.71 MPa, and stress in section 3-3 was mainly distributed between −3.60 MPa and −0.94 MPa, which was lower than that in the steel beam. All the above sections met the requirements of the Code for the Design of Highway Reinforced Concrete and Prestressed Concrete Bridges and Culverts of China, which stipulates that tensile stress be less than 1.15 times the standard tensile strength, 3.15 MPa, and that compressive stress be less than 0.7 times the standard compressive strength, 24.8 MPa, under construction loading. However, the stress situation of the concrete in the joint was more complicated. Section 3-3 was near the anchorage position of the prestressing tendons in the front bearing plate, and the stress concentration appeared in the web. The stress distribution in section 3-3 from Figure 7 is shown in Figure 18.

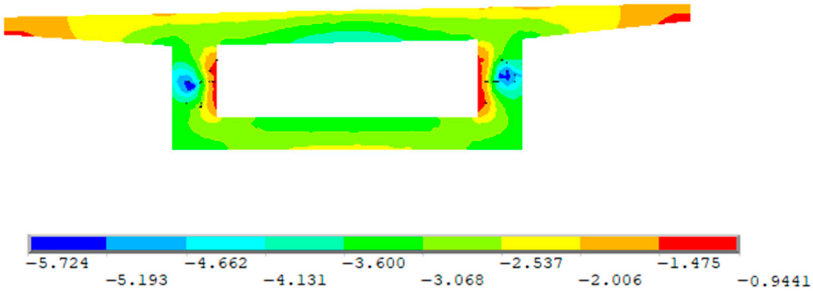

Figure 18. Stress distribution of concrete section 3-3 (MPa).

Figure 19 shows the measured and calculated stresses of concrete in sections 8-8 and 9-9 from Figure 7, respectively. As shown in the figures, the errors between the measured and calculated values of the top and bottom slabs of sections 8-8 and 9-9 in the parallelogram direction did not exceed 10%, which indicated that the fitting model was proper. The stress in the top plate of section 8-8 tended to decrease from the center line of the beam to the outer edge of the section, while the stress in the bottom plate tended to increase from the center line of the beam to the outer side of the web. The maximum difference between the measured and calculated values of top and bottom plate stresses were 0.21 MPa and 0.17 MPa, respectively. The stress in the top plate of section 9-9 increased and then decreased from the centerline of the beam to the outer edge of the section, while the stress in the bottom plate was evenly distributed near the centerline of the beam and gradually increased near the web. The maximum difference between the measured and calculated values of top and bottom plate stresses were 0.12 MPa and 0.26 MPa, respectively. Along the longitudinal direction of the bridge span, the stresses in the top and bottom slabs of the concrete structure gradually increased from sections 8-8 to 9-9.

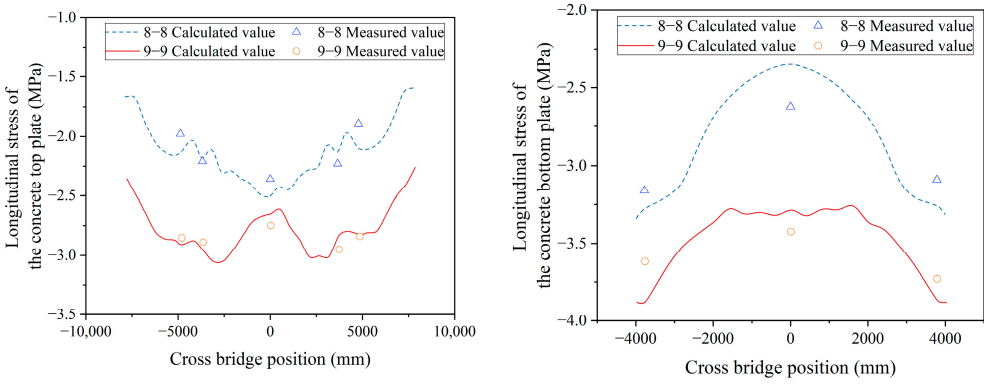

Figure 19. Transverse distribution of concrete stress in cross sections (MPa). (**a**) Concrete top plate stress. (**b**) Concrete bottom plate stress.

6. Conclusions

In this paper, the mechanical performance of the main beam and joint was analyzed through on-site construction monitoring combined with finite element calculation results, and the conclusions are as follows:

(1) In the hoisting of the mid-span closed steel beam, the side span of the main beam was stretched up while the middle span was stretched down, and the deformation was large, which should be taken as the key construction control condition.

(2) The calculated values of the finite element model and fine model of the joint of the hybrid beam bridge in the construction stage were in good agreement with the measured values. During the hoisting of the mid-span closing steel beam, the maximum difference between the calculated and measured values of the main beam deflection was not more than 5 mm, and the difference between the measured and calculated values of the stress variation of the top and the bottom plate was not more than 0.3 MPa. The error between the calculated and measured values of the fine model of the joint was not more than 15%.

(3) During the hoisting of the mid-span steel beam, the joint steel structure was under pressure as a whole. The longitudinal stress of the steel structure along the bridge gradually decreased from the front bearing plate section to the steel–concrete joint surface. The transverse stress distribution of the top plate was complicated and was different at different sections, but the transverse stress distribution of the bottom plate had a clear law whereby the stress increased gradually from the beam centerline to the stiffened web and decreased rapidly from the stiffened web to the edge of the bottom plate.

(4) The concrete at the joint was under compression, and the overall level of compressive stress was low when the mid-span steel beam was hoisted. The longitudinal stress of the concrete structure along the bridge gradually increased from the front bearing plate section to the steel–concrete joint surface. The compressive stress at the outer edge of the section of the concrete top plate with the same cross-section was the minimum, and the compressive stress at the junction between the bottom plate and the web was the maximum. There was a phenomenon of stress concentration near the anchorage point of the prestressed reinforcement, but the level of concentrated stress was low.

Author Contributions: Conceptualization, H.P. and L.J.; methodology, H.P. and L.J.; validation, H.P. and L.J.; formal analysis, H.P. and L.J.; investigation, H.P. and R.X.; data curation, J.L. and K.L.; writing—original draft preparation, K.L.; writing—review and editing, L.J. and J.L.; visualization, J.L.; supervision, L.J. and R.X.; project administration, L.J. and R.X.; funding acquisition, L.J. All authors have read and agreed to the published version of the manuscript.

Funding: This research was funded by the National Natural Science Foundation of China, grant number 51878488. Jiangxi Provincial Department of Communications Fund Project (2022H0019).

Data Availability Statement: The data of this study are available from the corresponding author upon reasonable request.

Acknowledgments: The authors sincerely thank the anonymous reviewers for their comments and suggestions for this article.

Conflicts of Interest: The authors declare no conflict of interest.

References

1. He, Z.-Q.; Chen, J.; Liu, Z.; Ma, Z.J. An Explicit Approach for Determining the Rational Length of Steel Portion in Steel-Concrete Hybrid Girder Bridges. *J. Bridge Eng.* **2023**, *28*, 5022011. [CrossRef]
2. Liu, R.; Yu, J.; Liu, Y.; Wu, D. Mechanical Analysis of Joint Sections of Hybrid Girder of Edong Changjiang River Bridge. *Bridge Constr.* **2010**, *33–35*, 62.
3. Shen, Q.; Shao, J.; Xu, J.; Yu, L.; He, X. Study of Force Transmitting Behavior of Joint Section of a Three-Span Steel and Concrete Continuous Hybrid Girder Bridge. *Bridge Constr.* **2012**, *42*, 70–74.
4. He, W.; Liu, Y.; Wang, R. Analysis of Joint Section Structure of Hybrid Girder of Jiujiang Changjiang River Highway Bridge. *Bridge Constr.* **2012**, *42*, 30–35.
5. Chen, K.; Wang, J.; An, Q. Model tests on steel-concrete joining section of main girder of a cable-stayed bridge. *China Civ. Eng. J.* **2006**, *39*, 86–90.

6. Huang, C.; Zhang, Z.; Chen, K. Model Test and Transfer Mechanism of Steel-Concrete Composite Structure for Hybrid Girder Cable-Stayed Bridges. *J. Huazhong Univ. Sci. Technol. Nat. Sci.* **2012**, *40*, 67–71.
7. Qin, F.; Di, J.; Dai, J.; Lu, W.; Zhao, M. Study on Rational Position of Joint Section of Steel-Concrete Hybrid Girder Bridge. In *Proceedings of the Construction and Urban Planning, Pts 1–4*; Huang, Y., Bao, T., Wang, H., Eds.; Trans Tech Publications Ltd.: Stafa-Zurich, Switzerland, 2013; Volume 671–674, pp. 1007–1011.
8. Qin, F.; Zhou, X.; Liang, B.; Di, J.; Tu, X.; Xu, L.; Zou, Y. Experiment on Steel-Concrete Joint of Hybrid Girder of a Long-Span Self-Anchored Suspension Bridge. *China J. Highw. Transp.* **2018**, *31*, 52–64.
9. Yao, Y.; Yang, Y.; Liu, Z.; Shi, Z.; Pu, Q. Model Tests on the Steel-Concrete Joint Section of Hybrid Cable-Stayed Railway Bridge with Long-Span Steel Box Girder. *J. China Railw. Soc.* **2015**, *37*, 079–084.
10. Cheng, X.; Nie, X.; Fan, J. Structural Performance and Strength Prediction of Steel-to-Concrete Box Girder Deck Transition Zone of Hybrid Steel-Concrete Cable-Stayed Bridges. *J. Bridge Eng.* **2016**, *21*, 4016083. [CrossRef]
11. Wei, F.; Luo, H.; Liang, L.; Xiao, Y.; Su, C. Mechanical Performance Analysis of Steel-Concrete Joint Section of a Long-Span Hybrid Girder Cable-Stayed Bridge Based on Field Test. *J. Chang. Univ. Nat. Sci. Ed.* **2021**, *41*, 54–65.
12. Kulkarni, S.A.; Li, B.; Yip, W.K. Finite Element Analysis of Precast Hybrid-Steel Concrete Connections under Cyclic Loading. *J. Constr. Steel Res.* **2008**, *64*, 190–201. [CrossRef]
13. Zhang, G.; Chen, C.; Liu, Y. Load Transfer Mechanism Between Cells and Bearing-Plate in Hybrid Girder Joint. *J. Tongji Univ. Nat. Sci.* **2017**, *45*, 658–663.
14. Kim, S.-H.; Lee, C.-G.; Ahn, J.-H.; Won, J.-H. Experimental Study on Joint of Spliced Steel–PSC Hybrid Girder, Part I: Proposed Parallel-Perfobond-Rib-Type Joint. *Eng. Struct.* **2011**, *33*, 2382–2397. [CrossRef]
15. Kim, S.-H.; Lee, C.-G.; Kim, S.-J.; Won, J.-H. Experimental Study on Joint of Spliced Steel–PSC Hybrid Girder, Part II: Full-Scale Test of Spliced Hybrid I-Girder. *Eng. Struct.* **2011**, *33*, 2668–2682. [CrossRef]
16. Xin, H.; Liu, Y.; He, J.; Zhang, Y. Experimental and Analytical Study on Stiffened Steel Segment of Hybrid Structure. *J. Constr. Steel Res.* **2014**, *100*, 237–258. [CrossRef]
17. Liu, R.; Liu, Y. Analysis of Auxiliary Ribs in Steel–Concrete Joint of Hybrid Girder. *J. Constr. Steel Res.* **2015**, *112*, 363–372. [CrossRef]
18. He, J.; Liu, Y.; Pei, B. Experimental Study of the Steel-Concrete Connection in Hybrid Cable-Stayed Bridges. *J. Perform. Constr. Facil.* **2014**, *28*, 559–570. [CrossRef]
19. He, S.; Fang, Z.; Fang, Y.; Liu, M.; Liu, L.; Mosallam, A.S. Experimental Study on Perfobond Strip Connector in Steel-Concrete Joints of Hybrid Bridges. *J. Constr. Steel Res.* **2016**, *118*, 169–179. [CrossRef]
20. He, S.; Fang, Z.; Mosallam, A.S. Push-out Tests for Perfobond Strip Connectors with UHPC Grout in the Joints of Steel-Concrete Hybrid Bridge Girders. *Eng. Struct.* **2017**, *135*, 177–190. [CrossRef]
21. He, S.; Mosallam, A.S.; Fang, Z.; Liu, L. Structural Evaluation of Steel-Concrete Joint with UHPC Grout in Single Cable-Plane Hybrid Cable-Stayed Bridges. *J. Bridge Eng.* **2019**, *24*, 4019022. [CrossRef]
22. Liu, Q.; Li, X.; Zhang, X.; Zhang, Z.; Li, Y. Stiffness Transition Analysis of a Steel-Concrete Joint Section Based on Vehicle-Bridge Interaction. *J. Southwest Jiaotong Univ.* **2013**, *48*, 810–817.
23. Li, C.; Lu, B.; Wang, C.; Peng, W. Dynamic Performance Assessment of a Novel Hybrid Bridge System with Spread Steel Box Girders. *J. Bridge Eng.* **2022**, *27*, 4021097. [CrossRef]
24. Zhang, X.; Zhang, S.; Niu, S. Experimental Studies on Seismic Behavior of Precast Hybrid Steel-Concrete Beam. *Adv. Struct. Eng.* **2019**, *22*, 670–686. [CrossRef]
25. Lu, B.; Zhai, C.; Li, S.; Wen, W. Predicting Ultimate Shear Capacities of Shear Connectors under Monotonic and Cyclic Loadings. *Thin-Walled Struct.* **2019**, *141*, 47–61. [CrossRef]